Neutron scattering from elemental indium: Optical model and bound-state potential

S. Chiba,* P. T. Guenther, R. D. Lawson, and A. B. Smith
Engineering Physics Division, Argonne National Laboratory, 9700 South Cass Avenue, Argonne, Illinois 60439
(Received 5 July 1990)

Neutron elastic-scattering cross sections of indium are measured from 4.5 to 10 MeV at intervals of ≈500 keV. Seventy or more differential values are obtained at each incident energy, distributed between ≈18° and 160°. These are combined with lower-energy data previously obtained at this laboratory, and with 11- and 14-MeV results from the literature, to form a comprehensive elastic-scattering database extending from ≈1.5 to 14 MeV. These data are interpreted in terms of a conventional spherical optical model. The resulting potential is extrapolated to the bound-state regime. It is shown that in the middle of the 50–82 neutron shell, the potential derived from the scattering results adequately describes the binding energies of particle states, but does not do well for hole states. The latter shortcoming is attributed to hole states having occupational probabilities sufficiently different from unity so that the exclusion principle becomes a factor, to rearrangement of the neutron core, and to the fact that the shell-model potential was assumed to have an energy-independent geometry. The systematic behavior of the real optical potential is discussed, and it is shown that the isovector strength deduced from neutron scattering is consistent with the nucleon-nucleon scattering data when a mass dependence of the radius is used.

I. INTRODUCTION

Over the past few years, we have extensively studied neutron scattering and total cross sections of a number of nuclei over the energy range of ≈1.5–10 MeV.[1–5] This energy range is rewarding since it is broad enough to reasonably define the average energy-dependent trends of the optical model (OM) in a region where there are expected to be changes, it adjoins the bound-state regime, and it is sensitive to nuclear-structure effects that largely average out at higher energies where many more reaction channels are open. Up until now emphasis has been given to nuclei near shell closures (i.e., A approximately equal to 90 and 208), and to nuclei in the $A=50$–60 region, where the nucleon configuration outside shell closures is relatively simple. This work has shown that, in these cases, it is possible to obtain a reasonable degree of unification of potentials applicable to bound and unbound energy regimes by means of the fundamental dispersion relationship.[6] The results also suggest that the real portion of the optical potential behaves in a rather smooth manner with target mass, but that the imaginary portion of the interaction is quite specific to the particular target, being sensitive to structure properties such as the number of particles (or holes) beyond a shell closure, and to collective motions. The present investigation extends this work to a region well away from a shell closure where the particle (hole) configurations are no longer simple. Previous knowledge of fast-neutron interactions with indium is sparse and largely confined to the lower-energy results obtained at this laboratory.[7,8] The present work builds upon and extends the prior results in order to provide an energy scope that permits an assessment of the optical potential and its relationship to the bound-state regime away from the shell closures.

In the present work, the neutron elastic-scattering cross sections of indium were measured, in detail, from ≈4.5 to 10 MeV using the methods outlined in Sec. II. The results of these measurements are given, and compared with previously reported values, in Sec. III. A spherical optical model (SOM) interpretation of these data, and the resulting model parameters, are given in Sec. IV. The extrapolation of this SOM to the bound-state regime is discussed in Sec. V. Systematic mass trends of the real potential (particularly the radius) and the correlation of nucleon-nucleon scattering data with the real strength of the SOM derived in the present and related[1–5] work are discussed in Sec. VI.

II. EXPERIMENTAL METHODS

All of the present measurements were made using the Argonne ten-angle fast-neutron time-of-flight apparatus.[9] Since the method, the apparatus, and the data acquisition and reduction have been described in detail elsewhere,[9–11] only an outline is given here.

The neutron source was the $D(d,n)^3He$ reaction, with the deuterium target gas contained in a cell 3 cm long.[12] The gas pressure within the cell was adjusted to give incident-neutron energy spreads at the sample, including effects due to kinematics, of 100–200 keV. The mean energy of the incident neutrons was determined to within 25–50 keV by control of the incident deuteron beam. The neutron source was pulsed at a repetition rate of 2 MHz, with a burst duration of ≈1 ns. The scattering sample was a solid cylinder of elemental indium, 2 cm long and 2 cm in diameter. Ten hydrogenous scintillation detectors were placed at scattered-neutron flight paths of ≈5 m. The relative scattering angles were determined to <0.1°, and the absolute scale was calibrated to ±0.1° by observing neutrons scattered from the sample both left and right of the apparent geometric center line, at angles where the elastic-scattering cross section is rap-

idly changing. The relative detector energy-dependent sensitivities were determined using the ^{252}Cf fission-neutron spectrum, as described in Ref. 13. These relative sensitivities were then normalized to the well-known H(n,n) scattering standard[14] by observing neutrons scattered from polyethylene (CH_2) samples. The measured cross sections were corrected for multiple-event, incident-beam-attenuation and angular-resolution perturbations using Monte Carlo techniques.[15] These calculations were carried through three iterations so as to provide an accuracy of 1–2 % at most angles. However, at the very minima of the distributions (in the range 35°–45°, a very deep and narrow minimum occurs at some energies), the uncertainties in the correction factors may be 30% or more. The detector calibrations were reproducible to $\leq 3\%$ up to ≈ 8.5 MeV. Since the intensity of the ^{252}Cf fission spectrum falls rapidly as the emitted-neutron energy increases above ≈ 3 MeV, this reproducibility deteriorated to about 5% at higher incident energies. Counting statistics varied a great deal, depending on the magnitude of the cross section. At forward angles where the intensities are high, the statistical uncertainties are $< 1\%$, whereas at the very minima of the higher-energy distributions, where the counting rate was approximately three orders of magnitude smaller, the statistical uncertainties increased to 10% or more. The various uncertainty estimates were combined in quadrature to obtain the total uncertainty.

III. EXPERIMENTAL RESULTS

The differential neutron elastic-scattering cross sections of elemental indium (95.7% ^{115}In, 4.3% ^{113}In) were measured at ≈ 0.5 MeV incident-neutron-energy intervals from 4.5 to 10 MeV. Seventy or more differential values, distributed between $\approx 18°$ and 160°, were obtained at each incident energy. For each distribution the measurements were made at several different times, using independent calibrations, with good reproducibility of the results. At all scattering angles and incident energies, the scattered-neutron experimental resolution was not sufficient to resolve neutrons due to inelastic excitation of the 336.3-keV ($\frac{1}{2}^-$) metastable level[8] in ^{115}In (and the analogous level in ^{113}In). Therefore, the experimental resolution was intentionally kept to ≈ 500 keV, and thus inelastic scattering involving the first $\frac{1}{2}^-$ levels was included with the elastic contribution in all of the experimental observations. This inelastic-neutron component is not generally a concern in the present considerations, since, even at 3 MeV, the cross section for the excitation of the 336.3-keV level in ^{115}In is only ≈ 10 mb and is falling with energy.[16] Consequently, its contribution to the present measurements is probably less than a mb/sr, which is smaller than the experimental uncertainty associated with the observations. Thus, in the present work, the observed cross sections are considered to be entirely due to elastic scattering.

The differential elastic-scattering cross sections resulting from the present measurements are shown in Fig. 1 (the 4.5–10-MeV energy range). These results reasonably extrapolate to the lower-energy values previously reported from this laboratory,[8] and, except at large scattering angles, to the 11.1-MeV results of Ferrer *et al.*[17] There are very few directly comparable previously reported elastic-scattering results. However, Holmqvist and Wiedling[18] have measured elastic-scattering cross sections at 4.56, 7.05, and 8.05 MeV. Their results are qualitatively consistent with those of the present work, as illustrated in Fig. 2.

IV. MODEL INTERPRETATION

The database considered in the model interpretation consisted of the following: (i) the s- and p-wave strength functions;[19] (ii) the neutron total cross section from a few keV to 20 MeV;[16] (iii) the elastic scattering of Ref. 8 from 1.5 to 3.8 MeV; (iv) the present elastic-scattering work extending from 4.5 to 10 MeV; (v) the 11.1-MeV elastic scattering of Ref. 17; and (vi) the 14.6-MeV elastic scattering of Ref. 20. The lower-energy data of Ref. 8 were averaged over 200-keV incident-energy increments in order to smooth any fluctuations, and to reduce the number of data points to manageable proportions for the fitting procedures. The total cross sections are shown in Fig. 3, and the composite elastic-scattering data used in

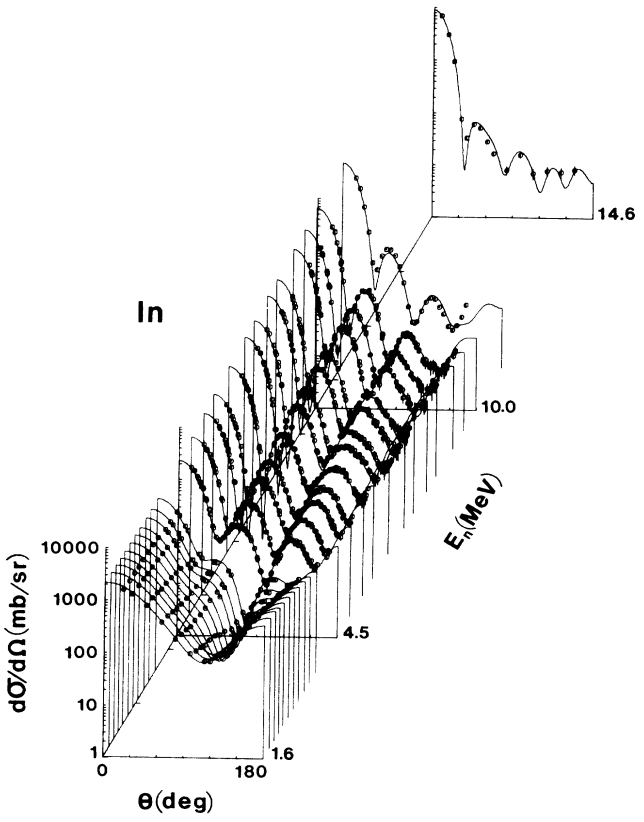

FIG. 1. Differential elastic-scattering cross sections of indium. Measured values are indicated by open circles. The present experimental results extend from 4.5 to 10 MeV, the 1.5–3.8-MeV results are from Ref. 8, the 11.1-MeV results from Ref. 17, and the 14.6-MeV results from Ref. 20. Curves indicate the results of model calculations as discussed in the text. The data are in the laboratory coordinate system.

the fitting are given in Fig. 1.

Since elemental indium is 95.7% ^{115}In, it was assumed that the target was monoisotopic ^{115}In. With this proviso, the data were analyzed using a conventional SOM having a real potential of the Woods-Saxon type, a Woods-Saxon-derivative imaginary interaction, and a spin-orbit (SO) term of the Thomas form.[21] A preliminary study indicated that the interpretation was not particularly sensitive to the spin-orbit parameters. Values of these parameters similar to those used in fitting the 1.5–3.8-MeV data,[8] and which give a reasonable description of the unpublished 4-MeV polarization results of Gorlov *et al.*,[22] were used:

$$V_{SO}=5.5 \text{ MeV} ,$$
$$r_{SO}=1.0 \text{ fm} , \quad (1)$$
$$a_{SO}=0.65 \text{ fm} ,$$

where V_{SO}, r_{SO}, and a_{SO} are, respectively, the strength, radius, and diffuseness of the Thomas term. (The nuclear radii R_i of the various constituents of the SOM potential are given by $R_i=r_i A^{1/3}$.)

With the spin-orbit potential held fixed to the values of Eq. (1), the remaining SOM parameters were determined by fitting the elastic-scattering database shown in Fig. 1. The procedures started with six-parameter chi-square fits in which the real and imaginary strengths, radii, and diffusenesses were varied. The levels[23] of ^{115}In up to a 1.5-MeV excitation energy were explicitly taken into account in the calculations using the Hauser-Feshbach[24] approach, corrected for resonance width fluctuations and correlations in the manner described by Moldauer.[25] Higher-energy excitations were incorporated into the calculations using the statistical formalism and parameters of Gilbert and Cameron.[26] It was further assumed that above 5 MeV the observed elastic scattering was entirely shape elastic, with no compound-elastic contributions. This is a reasonable assumption, in view of the very large level density at these higher energies.

The most stable parameter resulting from the six-parameter fitting was the real radius r_v, which decreased slightly with increasing energy. Over the 1.5–14.6-MeV energy range

$$r_v=(1.258-0.003E) \text{ fm} , \quad (2)$$

where the energy E is in MeV. The slope is very small and its relative uncertainty fairly large, so that the E variation is probably not significant. However, in the subsequent discussion, r_v, as given by Eq. (2), is used. (Throughout this paper, parameters are cited to a precision which makes accurate reproduction of the calculated results possible. We by no means imply that, for example, the nuclear radius has been determined accurately to three decimal places.)

The fitting procedure was repeated using a five-parameter chi-square search, varying real and imaginary strengths and diffusenesses, and the imaginary radius. Of the resulting five parameters, the real diffuseness a_v appeared the most stable and showed no significant energy dependence. Therefore, the a_v results of the fitting procedure were averaged to obtain the value

$$a_v=0.6404 \text{ fm} . \quad (3)$$

This value was accepted for the subsequent SOM fitting procedures.

Using the parameters of Eqs. (1)–(3), four-parameter fits were carried out. Although the imaginary diffuseness a_w may increase somewhat with energy, the slope is

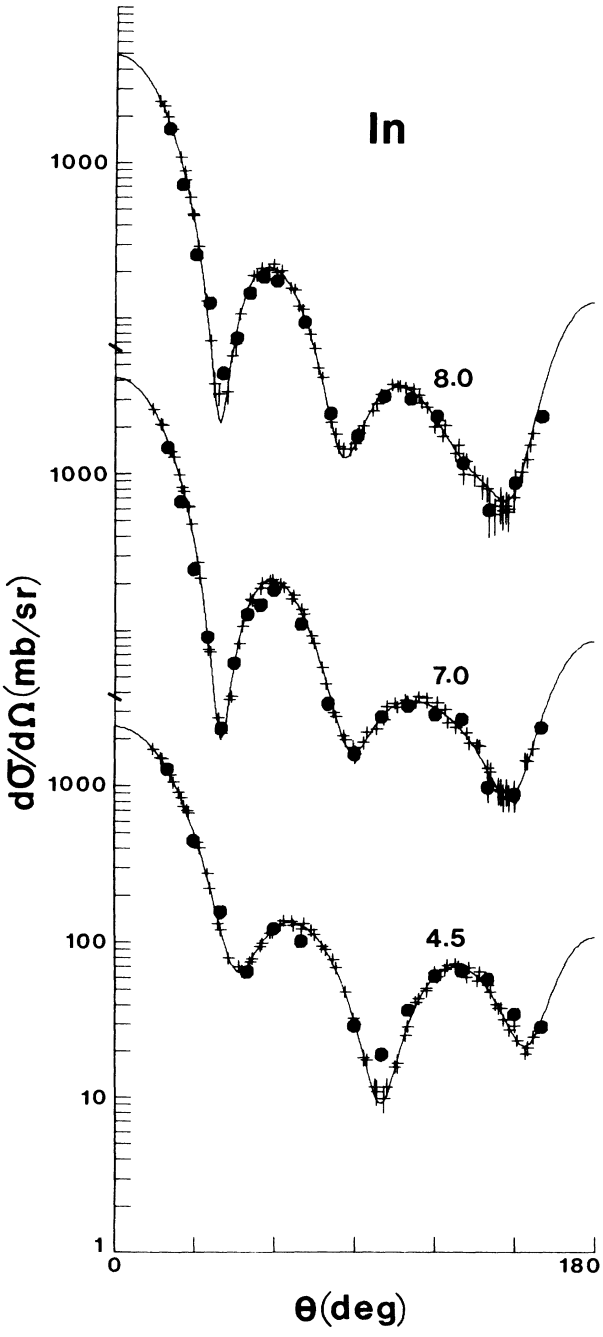

FIG. 2. Comparison of the present elastic-scattering cross sections (+) with those given in Ref. 18 (●). Curves are guides for the eye. Approximate energies are given in MeV. The data are in the laboratory coordinate system.

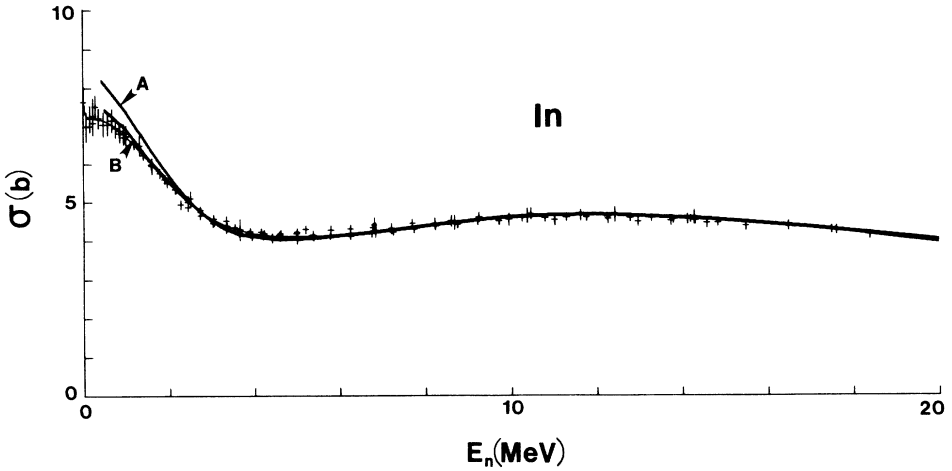

FIG. 3. Indium total cross sections. The data symbols are energy-averaged experimental values from Ref. 16. The light curve indicates the evaluation of Ref. 16. The heavy curves A and B show the results of model calculations as described in the text.

small, and a_w was taken to be constant with energy, having the value

$$a_w = 0.5798 \text{ fm} . \quad (4)$$

This value was then used in three-parameter fitting from which the imaginary radius r_w was selected to be

$$r_w = (1.305 - 0.003E) \text{ fm} , \quad (5)$$

where the small energy dependence was chosen equal to that of r_v.

Finally, two-parameter fitting, with the other parameters taken from Eqs. (1)–(5), resulted in the real and imaginary potential strengths

$$J_v = (433.4 - 3.7E) \text{ MeV fm}^3 \quad (6)$$

and

$$J_w = (41.8 + 2.9E) \text{ MeV fm}^3 , \quad (7)$$

where J_v and J_w are the volume integrals per nucleon of the real and imaginary potentials, respectively. The energy dependence of J_v and J_w is shown in Figs. 4 and 5, respectively. Uncertainties associated with J_v and J_w are hard to determine, since they are related by complex error propagation to the difficult-to-determine errors in the underlying database, particularly in dealing with results other than the present measurements. The uncertainties shown in Figs. 4 and 5, 1% for J_v and 5% for J_w, seem consistent with the scatter of the individual values.

Equations (1)–(7) define a SOM for the interaction of fast neutrons with indium. The model provides a very good description of the total cross section from 1.5 to 20 MeV, as illustrated in Fig. 3. The calculated total cross sections are consistent with the experimentally based evaluation of Ref. 16 to within 2%; i.e., to within approximately the uncertainty in the evaluation alone. This SOM also gives a reasonably good description of the present differential elastic-scattering results, as illustrated in Fig. 1. The only major differences are in the depth of the first minimum of the distributions in the energy range ≈ 6–8 MeV. The calculated minimum is very deep and narrow, changing by more than an order of magnitude over an angular range of 3°–4°. Such a "spikelike" behavior is difficult to observe without a specialized experiment. The SOM describes the lower-energy, 1.5–3.8-MeV, measured elastic scattering of Ref. 8 very well, as illustrated in Fig. 1. Furthermore, it reproduces the rather featureless 0.3–1.5-MeV elastic-scattering distributions previously reported from this laboratory.[7]

Turning to the higher-energy data, the present SOM reproduces the 11.1-MeV results of Ref. 17, except at large scattering angles. On the other hand, the rather rapid rise in this 11.1-MeV cross section at back angles, shown in Fig. 1, seems to be inconsistent with what one would expect from an extrapolation of the 10-MeV data. Finally, this SOM quite reasonably describes the 14.6-MeV data of Ref. 20, as can be seen in Fig. 1. No improvement in the description of the higher-energy data was obtained by the introduction of a volume absorption term in the SOM potential.

Below 1.5 MeV, the SOM defined by Eqs. (1)–(7) tends to predict neutron total cross sections that are increasing-

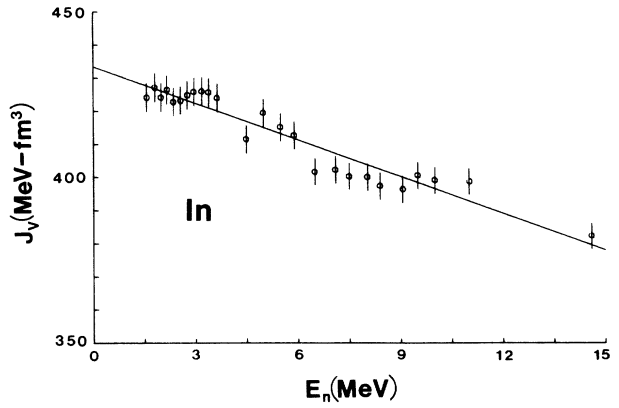

FIG. 4. The volume integral per nucleon J_v of the real potential resulting from the interpretation of the text. Symbols indicate the results of individual fits to the elastic-scattering data, while the curve indicates the least-square fit given by Eq. (6).

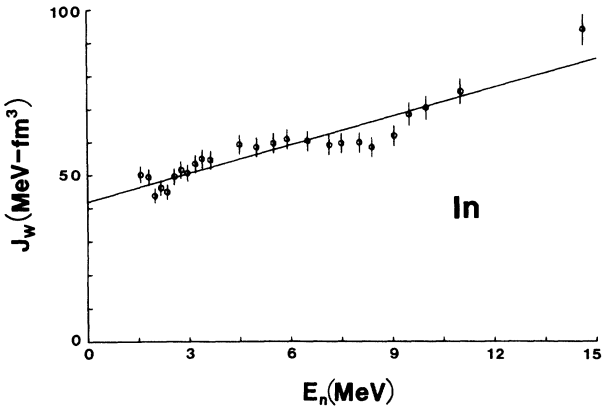

FIG. 5. The volume integral per nucleon J_w of the imaginary potential resulting from the interpretation described in the text. The notation is identical to that of Fig. 4, except that the curve is obtained from Eq. (7).

ly larger than those observed experimentally as the energy decreases, amounting to approximately a 10% overestimate at a few hundred keV. This trend is illustrated by curve *A* in Fig. 3. Some of this difference may be experimental, as the measured values were generally not corrected for self-shielding effects and thus may be several percent too small. Also, the predicted *s*- and *p*-wave strength functions are both approximately a factor of 2 larger than those deduced from resonance measurements.[19] However, it is commonly observed that the imaginary diffuseness a_w decreases to quite small values as the energy approaches zero,[1-5] rather than remaining constant as given by Eq. (4). The available experimental information does not permit a clear definition of this behavior in the case of indium. If one approximates the behavior by assuming that a_W decreases in a linear manner from the value of Eq. (4) at 2.0 MeV to 0.25 fm at zero energy, and J_W takes the values of Eq. (7), a reasonably good description of the observed neutron total cross sections at low energies is obtained, as illustrated by curve *B* in Fig. 3. In addition, *s*- and *p*-wave strength functions, in units of 10^{-4}, are now predicted to be 0.34 and 6.41, respectively, compared to the experimentally deduced values[19] of 0.26±0.03 and 3.2±0.6. Thus, decreasing a_W brings the *s*-wave strength function into good agreement with the experiment, but the calculated value of the more difficult to measure *p*-wave strength function is still a factor of 2 larger than deduced from resonance measurements. Finally, the potential scattering length R' is predicted to be 6.03 fm, in quite reasonable agreement with the experimental value[19] of (6.55±0.16) fm. Therefore, making a_W decrease, as one lowers the energy, substantially improves the agreement between the low-energy calculation and experiment. Moreover, this brings the SOM parameters into better agreement with those deduced from the lower-energy,[8] 1.5–3.8-MeV data alone.

V. BOUND-STATE PROPERTIES

There is a well-known dispersion relationship linking the real and imaginary OM potentials.[6] In this discussion, we shall use the fact that

$$J_V(E)=J_{\rm HF}(E)+\frac{\rm P}{\pi}\int_{-\infty}^{+\infty}\frac{J_W(E')}{E-E'}dE' , \tag{8}$$

where $J_V(E)$ and $J_W(E)$ are the volume integrals per nucleon of the total real and imaginary OM interactions, $J_{\rm HF}(E)$ is the Hartree-Fock component of the real potential, and P denotes the principal-value integral. Mahaux and Sartor[27,28] have exploited this relationship, together with similar expressions relating other radial moments of these interactions, to investigate the shell-model potential. The extrapolation to the bound-state regime gives an additional check on the consistency of the neutron OM potential, since it provides predictions concerning the binding energies of the shell-model states which were not considered in determining the scattering potential. The procedure is geared to finding the properties of single-particle states outside a closed shell, or single-hole states in a core. If the shell is not closed, the Pauli exclusion principle will "get in the way" in the prediction of, say, the single-particle energy ϵ_j of a j particle moving outside a partially filled j^n core. On the other hand, if the shell is only slightly occupied in the core, one might still hope to use the extrapolated potential to predict the single-particle energy, since the effect of the exclusion principle would be small. Because the pairing force favors occupation of the high j orbitals,[29] one might hope that near the middle of the $N=50-82$ shell, consisting of the $d_{5/2}$, $g_{7/2}$, $h_{11/2}$, $s_{1/2}$, and $d_{3/2}$ neutron orbitals, the low-spin states, $s_{1/2}$ and $d_{3/2}$, would have little population, and that their binding energies might be reasonably predicted by this extrapolation. In this section, we shall examine to what extent this is true for neutrons moving outside the $N=66$ (^{115}In) and $N=64$ (^{114}Sn) cores.

In order to use Eq. (8), J_W must be known for all energies. In the following calculations, the following is assumed.

(i) J_W is continuous and symmetric about the Fermi energy E_F.

(ii) For $2E_F \le E \le 0$, J_W is proportional to $(E-E_F)^2$.

(iii) For $0 \le E \le E_m$, J_W is given by Eq. (7). E_m is the energy at which this expression for J_W is equal to that obtained using Rapaport's[30] global parameters (for ^{115}In, $E_m=14.42$ MeV).

(iv) For $E_m \le E \le 30$ MeV, J_W has the linear energy dependence and values obtained using Rapaport's model.

(v) For $E \ge 30$ MeV, J_w is taken to be constant at its 30-MeV value.

With these assumptions, the contribution of the principal-value integral in Eq. (8) was evaluated and a best fit to the experimental values of $J_V(E)$, shown in Fig. 4, was made, assuming that

$$J_{\rm HF}=J_1+J_2E , \tag{9}$$

where J_1 and J_2 are constants.

The resulting expression for J_V is assumed to hold true for both positive and negative energies and, consequently, can be used to predict the real shell-model potential strength. In carrying out the OM fitting described in Sec. IV, it was found that the diffuseness of the real well, Eq.

(3), was energy independent. Furthermore, although a small energy dependence was found for r_V, Eq. (2), it is probably not significant, as noted above. Therefore, in discussing bound states, it is assumed that the shell-model potential has a constant diffuseness given by Eq. (3), and a constant radius $r_V = 1.258$ fm, the $E = 0$ value of Eq. (2). The shell-model spin-orbit potential is taken to be the Thomas form, described by the parameters of Eq. (1).

The single-particle energies for a neutron moving outside the ^{115}In core are difficult to determine, since the system is the odd-odd nucleus ^{116}In. The first and second excited states[31] of ^{116}In, which have I^π values of 5^+ and 4^+, show up strongly in stripping with an $l = 0$ pattern, and probably are the two possible spin states of a valence $s_{1/2}$ neutron coupling to the $\frac{9}{2}^+$ ground state of the ^{115}In core. Using the average energy of these two states, in conjunction with the binding-energy tables,[32] one concludes that the $s_{1/2}$ neutron is bound to the core by about 6.6 MeV. The next expected single-particle level would be the $d_{3/2}$, which can couple to ^{115}In to give spins ranging from 3^+ to 6^+. States with I^π values of 3^+, 4^+, 5^+, and 6^+ are seen in ^{116}In at excitation energies of 508 keV, 426 keV, 313 keV, and 649 keV, respectively. All except the 4^+ state show strong $l = 2$ stripping patterns. Unfortunately, none of the 4^+ states observed in the (d,p) reaction[31] show an $l = 2$ character, so that clear evidence for all states of the $(g_{9/2}^{-1}, d_{3/2})$ quartet cannot be found. On the other hand, a shell-model calculation using the Schiffer-True interaction[33] indicates that the 4^+ member of the quartet should lie about 120 keV about the 5^+ level, in good agreement with the observed 426-keV 4^+ state. Thus, using either the average of the four experimental energies quoted above, or using only the 3^+, 5^+, and 6^+ states, which exhibit $l = 2$ stripping patterns, one concludes that the $d_{3/2}$ single-particle orbit is bound by about 6.3 MeV to the ^{115}In core.

Since the $d_{5/2}$ and $g_{7/2}$ neutron states are the first to fill in the $N = 50$–82 region[34] and hold 14 particles, one might expect that the $\nu h_{11/2}$ state is not strongly populated in the core and, hence, the extrapolation procedure might provide a reasonable estimate of its energy. The $(\pi g_{9/2})^{-1}$ ground state of ^{115}In can couple with the $\nu h_{11/2}$ level to give spins ranging from 1^- to 10^-. Candidates for all these levels, except the 1^-, 2^-, and 10^- states, are seen in ^{116}In below 750 keV.[31] The average of these observed energies implies that the $h_{11/2}$ orbit is bound to the ^{115}In core by about 6.3 MeV. On the other hand, if one uses the Schiffer-True interaction[33] to predict the position of the other $(g_{9/2}^{-1}, h_{11/2})$ states, and combines them with the observed 3^- to 9^- levels, one finds that the binding energy to the core is about 5.9 MeV.

Assuming that the $g_{7/2}$ and $d_{5/2}$ orbits are full, one can learn about the binding of the hole states from ^{114}In. The ground-state spin of this nucleus[35] is 1^+, and is interpreted to arise from the $(\pi g_{9/2}^{-1}, \nu g_{7/2}^{-1})$ configuration. According to the Schiffer-True interaction,[33] this state lies about 1 MeV lower than the 2^+ member of the octet of states arising from this configuration, and more than 2 MeV lower than the other possible octet members, $I^\pi = 3^+$ to 8^+. If one uses the experimental energy of the 1^+ state alone, one concludes that the $g_{7/2}$ hole is bound by about 9 MeV to the ^{115}In core, whereas if one combines the 1^+ binding energy with the predicted Schiffer-True energies for the rest of the states in the multiplet, one obtains about 10.3 MeV for this binding. Finally, there is little evidence for the $(\pi g_{9/2}^{-1}, \nu d_{5/2}^{-1})$ sextet. The Schiffer-True interaction predicts that the lowest state would be 7^+, and there is some evidence for a 7^+ level at 642 keV in ^{114}In. If this is taken for the $d_{5/2}^{-1}$ energy, one concludes that the $d_{5/2}$ hole is bound by about 9.7 MeV. If the Schiffer-True potential is used to calculate the energies of all other spins of this configuration, and they are normalized to the yrast 7^+ level, one concludes that the $d_{5/2}$ hole-state binding energy is about 10.1 MeV.

The binding energies deduced from the experimental results alone and from the data, together with the Schiffer-True interaction, are shown in Table I. The well depths needed to give these binding energies are also shown in the table and are compared with the values pre-

TABLE I. Neutron binding energies (BE's) of the $s_{1/2}$, $d_{3/2}$, and $h_{11/2}$ particle states, and the $g_{7/2}$ and $d_{5/2}$ hole states relative to the ^{115}In and ^{114}Sn cores are tabulated. As discussed in the text, the position of the $d_{5/2}$ hole state in ^{114}In is very tenuous. In columns headed "experiment," only the observed states are considered. In the fourth column, the Woods-Saxon well depths needed to reproduce the BE's are shown when the diffuseness and radius are 0.6404 fm and 1.258 fm, respectively, and the spin-orbit potential is of the Thomas form with the parameters of Eq. (1). In the fifth column, the well depths predicted from the neutron-scattering analysis using Eq. (8) are given. Under the heading "Schriffer-True," the experimental data are augmented, as discussed in the text, to include the shell-model predictions for states of the various multiplets that have not been experimentally seen. For binding to the ^{114}Sn core only experimental data are used. All energies are in MeV.

			Experiment well depths	
Core	State	BE	Required	Predicted
^{115}In	$s_{1/2}$	6.6	45.1	45.5
	$d_{3/2}$	6.3	44.7	45.6
	$h_{11/2}$	6.3	47.3	45.6
	$g_{7/2}$	9.0	47.0	44.0
	$d_{5/2}$?	9.7	47.3	43.6
			Schiffer-True well depths	
Core	State	BE	Required	Predicted
^{115}In	$s_{1/2}$	6.6	45.1	45.8
	$d_{3/2}$	6.3	44.7	46.0
	$h_{11/2}$	5.9	46.8	46.2
	$g_{7/2}$	10.3	48.7	43.8
	$d_{5/2}$?	10.1	47.9	43.9
			Experiment well depths	
Core	State	BE	Required	Predicted
^{114}Sn	$s_{1/2}$	7.3	46.4	46.3
	$d_{3/2}$	6.9	45.8	46.5
	$h_{11/2}$	6.8	48.2	46.6
	$g_{7/2}$	10.4	49.0	44.8
	$d_{5/2}$	10.7	48.9	44.7

dicted by Eq. (8). In making these predictions, the Fermi energy E_F was taken to be

$$E_F=\tfrac{1}{2}(\epsilon_s+\epsilon_g)\ . \tag{10}$$

For the $s_{1/2}$, $d_{3/2}$, and $h_{11/2}$ particle states, the agreement between required and predicted well depths is reasonably good, the rms error being 1.1 MeV when the experimental results along are used, and 0.9 MeV when the data are augmented with the Schiffer-True predictions. This is similar to the rms deviation in ^{51}V, which was about 1.1 MeV when all the particle and hole states were included.[5] On the other hand, the required depths for the hole states are at least 3 MeV deeper than those predicted by Eq. (8).

To see whether or not the hole-state potential difference arises merely from the odd-odd nature of ^{116}In, the required well depths needed to explain the data in the neighboring odd-A tin isotopes were examined. Binding energies relative to the even-even ^{114}Sn nucleus can be obtained from a knowledge of the states in ^{113}Sn and ^{115}Sn. In this case, the 14 valence neutrons in the ^{114}Sn core are assumed to occupy the $(\nu d_{5/2})^6(\nu g_{7/2})^8$ configuration outside the closed $N=Z=50$ shell. The energies and spectroscopic factors given in the Nuclear Data Sheets[23] for ^{115}Sn allow one to obtain the single-particle energies defined by

$$\epsilon_j=\sum_i S_{ji}E_{ji}\Big/\sum_i S_{ji}\ , \tag{11}$$

where S_{ji} is the spectroscopic factor for populating the ith state with spin j and energy E_{ji}. Combining these results with the binding-energy tables[32] leads to the $s_{1/2}$, $d_{3/2}$, and $h_{11/2}$ particle-state energies, relative to ^{114}Sn, shown in Table I. In the same manner, the $g_{7/2}$ and $d_{5/2}$ energies are obtained from the data[36] on ^{113}Sn.

In order to use the ^{115}In scattering results to make predictions for well depths needed in ^{114}Sn, the following changes were made.

(i) According to Rapaport's global model,[30] the isovector contribution should change J_v in going from ^{115}In to ^{114}Sn by

$$\Delta J_v=(5.25-0.044E)\ \text{MeV fm}^3\ . \tag{12}$$

This contribution should be added to the J_v values shown in Fig. 4, so as to make them appropriate for ^{114}Sn.

(ii) Again using the global model,[30] one finds that $\Delta J_w=0.26$ MeV fm^3. Thus, for ^{114}Sn,

$$J_W=(42.06+2.9E)\ \text{MeV fm}^3\ . \tag{13}$$

Once these changes are made, the procedure is exactly as already discussed.

The results for the ^{114}Sn core are given in Table I. In the fourth column, the Woods-Saxon well depths required to give the observed binding energies are quoted. In the fifth column, the predicted well depths, found by use of Eq. (8) when the Fermi energy is given by Eq. (10), are listed. For particle states, the agreement between required and predicted well depths is quite reasonable, with the rms deviation between the two being about 1 MeV. However, once more, the well depths necessary to reproduce the hole-state energies are almost 10% greater than the values predicted by the use of Eq. (8).

Therefore, near the middle of the 50–82 neutron shell one concludes that when the OM potential found by fitting the indium scattering data is extrapolated to the bound-state regime, quite reasonable predictions can be made for the shell-model potential needed to give the experimental energies of the $h_{11/2}$, $d_{3/2}$, and $s_{1/2}$ particle states. On the other hand, this extrapolated potential cannot be used to predict the energies of the $d_{5/2}$ and $g_{7/2}$ hole states. At least three factors may contribute to the deficiency of the model for the hole states: First, an energy-independent geometry for the bound-state potential may be incorrect; second, the $d_{5/2}$ and $g_{7/2}$ levels may have an occupation probability sufficiently different from unity that the exclusion principle becomes a factor; and third, the core may change appreciably when the hole state is formed.

VI. DISCUSSION

Listed in Table II are the values of J_V and the radii r_V of the SOM potential appropriate for the scattering of 8-MeV neutrons from various nuclei, including the indium results presented in this paper. From an inspection of the table, it is clear that r_V decreases as the mass A

TABLE II. Values of r_v, J_v, r_w, and J_w obtained by fitting the data for the elastic scattering of 8-MeV neutrons from the nuclei listed in the first column. A spherical OM was assumed. The last two "systematics" columns give the values of r_v and J_v predicted with Eqs. (14), (15), and (17) of the text.

Nucleus and Ref.	Specific SOM				Systematics	
	r_v[a]	J_v[b]	r_w[a]	J_w[b]	r_v[a]	J_v[b]
^{51}V (5)	1.2680	440.4	1.2997	68.9	1.2667	451.3
^{58}Ni (46)	1.2538	462.9	1.2000	104.8	1.2617	461.7
^{59}Co (4)	1.2624	454.8	1.2119	85.6	1.2610	448.6
^{89}Y (2)	1.2400	424.5	1.3296	66.5	1.2465	423.9
^{90}Zr (47)	1.2593	431.9	1.3388	66.3	1.2461	426.6
^{93}Nb (1)	1.2500	426.3	1.3000	75.9	1.2451	423.7
^{115}In	1.2340	400.1	1.2810	65.0	1.2384	410.1
^{209}Bi (3)	1.2200	385.5	1.3102	43.0	1.2220	380.9

[a]Radii are given in fm.

[b]Volume integrals per nucleon J_i are given in MeV fm^3.

increases— a result similar to that found by Moldauer[37] when he attempted to fit very-low-energy neutron data. A least-squares fit was made to these radii assuming that

$$r_V = r_0 + r_1 / A^{1/3} , \tag{14}$$

in other words, assuming the nuclear radius R_V is proportional to $A^{1/3}$ plus a constant. When

$$r_0 = 1.1476 \text{ fm and } r_1 = 0.4416 \text{ fm} \tag{15}$$

the values listed under "systematics" in Table II are obtained. The fit to the empirically determined SOM radii is excellent, with an rms deviation between theory and experiment of approximately 0.5%. Furthermore, the values of r_0 and r_1 are similar to those given by Moldauer,[37] who obtained 1.16 fm and 0.6 fm, respectively, for these quantities.

In a similar way, J_V decreases as A increases. If one attempts to fit the empirical values with the relationship

$$J_V = J_0[1 - \xi(N-Z)/A] , \tag{16}$$

one finds $J_0 = 486.8$ MeV fm^3 and $\xi = 1.04$. These values are similar to those found by Holmqvist and Wiedling,[38] who also studied the scattering of 8-MeV neutrons from a number of nuclei and found $J_0 = 480$ MeV fm^3 and $\xi = 0.98$. They are also quite close to the 11.1-MeV results of Ferrer, Carlson, ad Rapaport[17] who obtained $J_0 = (495 \pm 30)$ MeV fm^3 and $\xi = 0.95$. On the other hand, the nucleon-nucleon scattering data indicate that ξ should be[39] about 0.48, and the (p,n) results are consistent[40] with a value of $\xi = 0.4$, both about a factor of 2 smaller than obtained from the analysis of the 8- and 11-MeV neutron-scattering data. However, the neutron-scattering results can be brought into reasonable agreement with the (p,n) and two-body data if one takes into account the radius variation proposed in Eq. (14). If one sets

$$J_V = K_0[1 - \xi(N-Z)/A](r_0 + r_1/A^{1/3})^3 , \tag{17}$$

with r_0 and r_1 having the values given in Eq. (15), one finds $K_0 = 234.2$ MeV and $\xi = 0.53$. The fit obtained in this way, and given in Table II, leads to a rms deviation between calculated and observed values of J_V of 6.3 MeV fm^3, the same as obtained when the conventional fit, Eq. (16), is made.

Thus, the real SOM potential obtained from the indium data fits in quite nicely with the values obtained from the study of other nuclei throughout the Periodic Table. Furthermore, the indium value of $a_V = 0.6404$ fm is similar to the average value, 0.67 fm, for the other nuclei listed in Table II.

In Table II, r_w and J_w, the radius and volume integral per nucleon of the imaginary SOM potential at 8 MeV, are also given. There is no evidence for a smooth variation of these quantities with mass number A, and this is consistent with the fact that the imaginary portion of the SOM is expected to be sensitive to nuclear structure. The values of J_w can, however, be divided into three groups: (i) $J_w < 50$, (ii) $50 < J_w < 80$, and (iii) $J_w > 80$ MeV fm^3. The only nucleus in this list in category (i) is ^{209}Bi. It is a doubly-closed-shell-plus-one nucleus, and the small value of J_w is consistent with the fact that the ^{208}Pb core is a very stable structure. Indium falls in the second group, which includes ^{51}V, ^{89}Y, ^{90}Zr, and ^{93}Nb. The first three members of this group can be adequately described by the spherical shell model,[41,42] and this implies that the low-lying states in ^{93}Nb and ^{115}In should also be understandable in terms of this model. For nuclei in this group, the cores are more easily excited than those near the doubly closed $Z = 82$, $N = 126$ shell and, consequently, J_w is larger. Finally, the two nuclei with $J_w > 80$ MeV fm^3 (namely, ^{58}Ni and ^{59}Co) not only have anomalously large values of J_w, but they also differ from other imaginary SOM potentials in two significant respects: (i) in the energy range $0 < E < 10$ MeV, J_w decreases as the incident energy increases, and (ii) $r_w < r_v$. These effects could imply that one is attempting to describe a deformed nucleus with a SOM.[4,43]

Thus, the imaginary SOM potential for indium has a J_w value consistent with other spherical nuclei. Furthermore, the empirical value of r_w for indium is only slightly larger than the average value, 1.3157 fm, obtained for other nuclei in this class. The diffuseness a_w of the derivative Woods-Saxon interaction varies significantly for the six nuclei considered to be spherical, ranging from 0.3933 fm for ^{89}Y to 0.5798 fm for indium. The imaginary diffuseness obtained for indium is about 0.12 fm greater than the average for the other spherical nuclei and, undoubtedly, this reflects differences in the nuclear structure.

In extrapolating the OM to the bound-state regime, only the volume integral per nucleon of the imaginary interaction was used, and attention was not given to the detailed form of the potential. For the so-called particle states, $s_{1/2}$, $d_{3/2}$, and $h_{11/2}$, the extrapolated potential gave Woods-Saxon well depths in satisfactory agreement with those needed to reproduce the observed binding energies. As pointed out in Sec. IV, the scattering data fitted in our interpretations were not particularly sensitive to the spin-orbit interaction. However, with the exception of the $s_{1/2}$ level, the binding energies are quite sensitive to this potential. For example, if one merely increases V_{SO} from 5.5 to 6.0 MeV, the required well depths needed to reproduce the observed binding of the $d_{3/2}$ and $h_{11/2}$ states to the ^{114}Sn core become 46.0 MeV and 47.9 MeV, respectively, and this reduces the rms deviation between the required and predicted well depths from 1.0 to 0.8 MeV. Thus, the bound particle states seem to indicate a slightly stronger spin-orbit potential than that deduced from neutron-scattering data.

Turning to the $d_{5/2}$ and $g_{7/2}$ hole states, the extrapolated OM potential does not explain their observed binding energies. Because of the lack of scattering data at higher energies, the global model of Rapaport[30] was used to evaluate the dispersion contribution to J_v, Eq. (8), and it was assumed that the Woods-Saxon well describing the bound-state potential had energy-independent geometry. If more data were available one could proceed *à la* Mahaux and Sartor[27,28] and try to deduce the energy variation of r_v and a_v to see if this would explain the hole-state data. Alternatively, one can examine the

changes in these parameters needed to explain the binding energies when J_v is held fixed at the value predicted by use of the scattering data and Rapaport's global model ($J_v \simeq 414$ MeV fm^3 for both the $g_{7/2}^{-1}$ and $d_{5/2}^{-1}$ states in ^{114}Sn.) If r_v is held fixed at 1.258 fm, then in order to obtain the observed hole-state binding energies, one must use $a_v \simeq 0.46$ fm and 0.37 fm for $g_{7/2}^{-1}$ and $d_{5/2}^{-1}$, respectively. At best, this is almost a 30% decrease in a_v from the scattering value and, moreover, Δa_v between the two states, which differ in binding by only 300 keV, is approximately 0.09 fm. Thus, the failure of the model for hole states is unlikely to be due to an energy dependence of a_v alone. On the other hand, if a_v is held fixed at 0.6404 fm and r_v is allowed to vary, a value of $r_v \simeq 1.17$ fm gives the observed binding of the $g_{7/2}^{-1}$ and $d_{5/2}^{-1}$ states when $J_v \simeq 414$ MeV fm^3. Consequently, a decrease of about 7% in r_v for the hole states compared to the particle states would reconcile the model with experiment. This change is somewhat greater than seen in either the ^{51}V case[5] or in the ^{208}Pb analysis,[44] but is not completely out of the question.

There are at least two other possible explanations as to why the energy-independent-geometry model fails for the hole states. First, the Pauli exclusion principle "gets in the way," and, second, the core configuration is changed when the hole state is produced. To check this, the ^{115}In OM potential was extrapolated to the ^{132}Sn nucleus by using Rapaport's[30] global values for the isovector potential strengths. In addition, since J_w is, in first order, proportional to $A^{-1/3}$, Eq. (7) was scaled by the factor $(115/132)^{1/3}$. The energies of the hole states in ^{131}Sn have been deduced by Fogelberg and Blomqvist,[45] and when these data are combined with the binding-energy tables,[32] one finds that the required well depths for the $d_{3/2}^{-1}$, $h_{11/2}^{-1}$, $s_{1/2}^{-1}$, $d_{5/2}^{-1}$, and $g_{7/2}^{-1}$ states are 42.8 MeV, 44.9 MeV, 43.3 MeV, 43.0 MeV, and 44.4 MeV, respectively. These are to be compared with the values predicted by use of Eq. (8), when $E_F = -6.5$ MeV, of 43.5, 43.4, 43.4, 42.9, and 42.6 MeV. Thus, the rms deviation between predicted and required well depths is about 1.1 MeV, the same as that found[5] for ^{51}V. Undoubtedly, the correct explanation of the bound-state problem is a combination of the effects discussed in this and the preceding paragraph. The fact that the energy-independent-geometry model works so well for ^{131}Sn would seem to indicate that an energy dependence of r_v and/or a_v is less important than the exclusion principle and rearrangement of the core.

This work was supported by the U.S. Department of Energy under Contract No. W-31-109-ENG-38.

---

*Visiting scientist from the Japan Atomic Energy Research Institute, Tokai Establishment, Tokai-mura, Japan.

[1]A. B. Smith, P. T. Guenther, and R. D. Lawson, Nucl. Phys. **A455**, 344 (1986).

[2]R. D. Lawson, P. T. Guenther, and A. B. Smith, Phys. Rev. C **34**, 1599 (1986).

[3]R. D. Lawson, P. T. Guenther, and A. B. Smith, Phys. Rev. C **36**, 1298 (1987).

[4]A. B. Smith, P. T. Guenther, and R. D. Lawson, Nucl. Phys. **A483**, 50 (1988).

[5]R. D. Lawson, P. T. Guenther, and A. B. Smith, Nucl. Phys. **A493**, 267 (1989).

[6]G. R. Satchler, *Direct Nuclear Reactions* (Clarendon, Oxford, 1983).

[7]W. G. Vonach and A. B. Smith, Nucl. Phys. **78**, 389 (1966).

[8]A. B. Smith, P. T. Guenther, and J. F. Whalen, Argonne National Laboratory Report ANL/NDM-78, 1982; see also A. Smith, P. Guenther, J. Whalen, I. Van Heerden, and W. McMurray, J. Phys. G **11**, 125 (1985).

[9]A. Smith, P. Guenther, R. Larson, C. Nelson, P. Walker, and J. Whalen, Nucl. Instrum. Methods **50**, 277 (1967).

[10]C. Budtz-Jorgensen, P. Guenther, A. Smith, J. Whalen, W. McMurray, M. Renan, and I. Van Heerden, Z. Phys. A **319**, 47 (1984).

[11]P. Guenther, A. Smith, and J. Whalen, Phys. Rev. C **12**, 1797 (1976).

[12]M. Drosg, IAEA Report IAEA-TECDOC-410, 1987, p. 239.

[13]A. Smith, P. Guenther, and R. Sjoblum, Nucl. Instrum. Methods **140**, 397 (1977).

[14]Nuclear Standards File, IAEA Technical Report 227, 1983, edited by H. Condé, A. Smith, and A. Lorenz.

[15]A. B. Smith, MONTE–SPHERE and MONTE–POLY, Monte Carlo correction codes (unpublished) (available from the author).

[16]A. B. Smith, S. Chiba, D. L. Smith, J. W. Meadows, P. T. Guenther, R. D. Lawson, and R. J. Howerton, Argonne National Laboratory Report ANL/NDM-115, 1990.

[17]J. C. Ferrer, J. D. Carlson, and J. Rapaport, Nucl. Phys. **A275**, 325 (1977).

[18]B. Holmqvist and T. Wiedling, Aktiebolaget Atomenergi Report AE-430, 1971.

[19]S. F. Mughabghab, M. Divadeenam, and N. E. Holden, *Neutron Cross Sections* (Academic, New York, 1981), Vol. 1, Part A.

[20]L. F. Hansen, F. S. Dietrich, B. A. Pohl, C. H. Poppe, and C. Wong, Phys. Rev. C **31**, 31 (1985).

[21]P. E. Hodgson, *Nuclear Reactions and Nuclear Structure* (Clarendon, Oxford, 1971).

[22]G. V. Gorlov, N. S. Lebedeva, and V. M. Morosov, private communication.

[23]J. Blachot and G. Marguier, Nucl. Data Sheets **52**, 565 (1987).

[24]W. Hauser and H. Feshbach, Phys. Rev. **87**, 366 (1952).

[25]P. A. Moldauer, Nucl. Phys. **A344**, 185 (1980).

[26]A. Gilbert and A. Cameron, Can. J. Phys. **43**, 1446 (1965).

[27]C. Mahaux and R. Sartor, Phys. Rev. Lett. **57**, 3015 (1986).

[28]C. Mahaux and R. Sartor, Nucl. Phys. **A484**, 205 (1988); see also references cited therein.

[29]L. S. Kisslinger and R. A. Sorensen, Rev. Mod. Phys. **35**, 853 (1963).

[30]J. Rapaport, Phys. Rep. **87**, 25 (1982).

[31]J. Blachot, J. P. Husson, J. Oms, G. Marguier, and F. Hass, Nucl. Data Sheets **32**, 287 (1981).

[32]A. H. Wapstra and K. Bos, At. Data Nucl. Data Tables **19**, 177 (1977).

[33]J. P. Schiffer and W. W. True, Rev. Mod. Phys. **48**, 191 (1976).

[34]E. J. Schneid, A. Prakash, and B. L. Cohen, Phys. Rev. **156**, 1316 (1967).
[35]J. Blachot and G. Marguier, Nucl. Data Sheets **35**, 375 (1982).
[36]J. Lyttkens, K. Nilson, and L. P. Ekstrom, Nucl. Data Sheets **33**, 1 (1981).
[37]P. A. Moldauer, Nucl. Phys. **47**, 65 (1963).
[38]B. Holmqvist and T. Wiedling, Nucl. Phys. **A188**, 24 (1972).
[39]G. W. Greenlees, W. Makofske, and G. J. Pyle, Phys. Rev. C **1**, 1145 (1970).
[40]C. J. Batty, E. Friedman, and G. W. Greenless, Nucl. Phys. **A127**, 368 (1969).
[41]R. D. Lawson, *Theory of the Nuclear Shell Model* (Clarendon, Oxford, 1980).
[42]S. Cohen, R. D. Lawson, M. H. Macfarlane, and M. Soga, Phys. Lett. **10**, 195 (1964).
[43]A. B. Smith, P. T. Guenther, and J. Whalen, Nucl. Phys. **A415**, 1 (1984).
[44]C. H. Johnson, D. J. Horen, and C. Mahaux, Phys. Rev. C **36**, 2252 (1987).
[45]B. Fogelberg and J. Blomqvist, Phys. Lett. **137B**, 20 (1984).
[46]A. B. Smith and P. T. Guenther (unpublished).
[47]S. Chiba, P. T. Guenther, R. D. Lawson, and A. B. Smith (unpublished).